Journal of Pharmacokinetics and Pharmacodynamics (2025) 52:16
https://doi.org/10.1007/s10928-025-09963-w

ORIGINAL PAPER

Reliability of in vitro data for the mechanistic prediction of brain extracellular fluid pharmacokinetics of P-glycoprotein substrates in vivo; are we scaling correctly?

Daan W. van Valkengoed[1] · Makoto Hirasawa[1] · Vivi Rottschäfer[2,3] · Elizabeth C. M. de Lange[1]

Received: 19 July 2024 / Accepted: 16 January 2025 / Published online: 8 February 2025

Abstract

Plasma pharmacokinetic (PK) profiles often do not resemble the PK within the central nervous system (CNS) because of blood–brain-border (BBB) processes, like active efflux by P-glycoprotein (P-gp). Methods to predict CNS-PK are therefore desired. Here we investigate whether in vitro apparent permeability (P_{app}) and corrected efflux ratio (ER_c) extracted from literature can be repurposed as input for the LeiCNS-PK3.4 physiologically-based PK model to confidently predict rat brain extracellular fluid (ECF) PK of P-gp substrates. Literature values of in vitro Caco-2, LLC-PK1-mdr1a/MDR1, and MDCKII-MDR1 cell line transport data were used to calculate P-gp efflux clearance (CL_{Pgp}). Subsequently, CL_{Pgp} was scaled from in vitro to in vivo through a relative expression factor (REF) based on P-gp expression differences. BrainECF PK was predicted well (within twofold error of the observed data) for 2 out of 4 P-gp substrates after short infusions and 3 out of 4 P-gp substrates after continuous infusions. Variability of in vitro parameters impacted both predicted rate and extent of drug distribution, reducing model applicability. Notably, use of transport data and in vitro P-gp expression obtained from a single study did not guarantee an accurate prediction; it often resulted in worse predictions than when using in vitro expression values reported by other labs. Overall, LeiCNS-PK3.4 shows promise in predicting brainECF PK, but this study highlights that the in vitro to in vivo translation is not yet robust. We conclude that more information is needed about context and drug dependency of in vitro data for robust brainECF PK predictions.

Keywords P-glycoprotein · PBPK · CNS · BBB · Pharmacokinetics · IVIVE

Introduction

Plasma pharmacokinetic (PK) profiles often do not resemble the PK within the central nervous system (CNS), which is mainly caused by the blood–brain-border (BBB) [1]. For compounds that exert their function within the central nervous system (CNS), the BBB poses a challenge, leading to high attrition rates observed for novel CNS drugs [2, 3]. Especially the efflux transporter P-glycoprotein (P-gp) plays a crucial role, as it limits a wide range of drugs in adequately accessing the brain [4, 5]. The complex interplay of passive diffusion, active transporters and intra-brain distribution makes PK profiles in the brain difficult to predict. A mechanistic and integrated understanding of the processes governing BBB transport is crucial for successful predictions of brain PK [6].

Information on the unbound drug PK in the brain extracellular fluid (brainECF), the target site of most CNS drugs, is required to understand the relationship between drug exposure and its effect, and to subsequently optimize therapy. The gold standard to measure this is through microdialysis that can be applied in animal studies, but is restricted in its use in humans due to ethical considerations [7]. Microdialysis studies allow us to improve mechanistic understanding of BBB transport, but animal studies are expensive and extensive (i.e., they are time-consuming and require technical expertise). Also, the use of animals should be restricted

✉ Elizabeth C. M. de Lange
ecmdelange@lacdr.leidenuniv.nl

[1] Division of Systems Pharmacology and Pharmacy, Leiden Academic Centre for Drug Research, Leiden University, Leiden, The Netherlands

[2] Mathematical Institute, Leiden University, Leiden, The Netherlands

[3] Korteweg-de Vries Institute for Mathematics, University of Amsterdam, Amsterdam, The Netherlands

where possible. Alternatively, in vitro models and assays hold promise for the prediction of drug penetration into the brainECF in vivo [8]. An example is the transwell permeability assay, used for the study of drug permeability across a monolayer of cells expressing transporters like P-gp [9, 10]. Mechanistic information on the interaction of a drug with a membrane and transporters can be derived from these assays, for prediction of BBB transport in vivo.

Multiple approaches using in vitro data to predict brain distribution of drugs have been published, including for P-gp substrates [11]. Most are focussed on the prediction of the extent of BBB transport, i.e. on $Kp_{uu,brain}$, which is the ratio of unbound drug concentration in the brain and that in plasma at steady state [12]. Summerfield et al. and Langthaler et al. showed, for example, how transport data from MDCKI/II cell lines could be used to predict $Kp_{uu,brain}$ in vivo [13, 14]. Similarly, Uchida et al. and Nicolaï et al. utilized LLC-PK1 cell line data to predict $Kp_{uu,brain}$ in mice, rats, and humans within threefold and twofold error, respectively, compared to observed $Kp_{uu.brain}$ [15, 16]. Measures of $Kp_{uu,brain}$ give important insights into the extent of drug distribution at steady state (SS), but neglect the importance of the rate of distribution and the processes before SS is reached [6, 17]. Since the receptor or target of interest is exposed to fluctuating concentrations of the drug over time after single doses or short infusions, the static, SS-measure of $Kp_{uu,brain}$ is not ideal to predict pharmacodynamic effect(s). In addition, the drug might have to compete with endogenous ligands at its target site, the success of which might change over the course of the treatment based on changing drug concentrations. Understanding and being able to predict a complete, temporal unbound PK profile is therefore crucial to relate drug doses to their ultimate effect.

For prediction of both the rate and extent of distribution, physiologically based pharmacokinetic (PBPK) models can be applied. They allow for predictions of PK profiles by leveraging physiological knowledge, drug-specific properties and mechanistic information from in vitro studies for predictions of drug PK in vivo [18]. Successful development of a generic CNS PBPK model that explicitly takes into account P-gp mediated clearance (CL_{Pgp}) at the BBB (and as such predicts both rate and extent of transport) is of significant interest. Such a model would have great potential for clinical applications but also for theoretical investigation, allowing what-if studies that explore P-gp activity specifically (e.g., to explore the impact of disease on P-gp functionality). Some PBPK models that use in vitro data to predict brain PK of P-gp substrates have already been developed [19–26]. Though informative, these models have a number of shortcomings: they (1) commonly rely on the introduction of empirical scaling factors to accurately predict observed data [19, 23, 24], (2) estimate additional transporters aside from P-gp which makes it hard to gauge the success of modelling P-gp [21, 26], and (3) often lay the focus on cerebrospinal fluid (CSF) instead of the more relevant brainECF [19, 24]. Moreover, these models have been validated with a limited number of drugs (no more than three drugs with temporal PK predictions, more often a single drug) [20–26], questioning their general applicability.

A large amount of literature is available on in vitro transport data. It makes sense from a 3R (Reduce, Recycle, Reuse*)* standpoint [27] to repurpose this data for PBPK models instead of setting up a new experimental study. An important factor that has not been investigated sufficiently in the context of CNS PBPK models is the variable nature of in vitro data [28, 29] that can impact the accuracy and robustness of model predictions [30, 31]. Understanding this impact is crucial, especially if an investigation relies on data retrieved from literature as starting point for a computational study. Therefore, it is still unclear to what extent the use of in vitro transport data as input in a CNS-PBPK model allows for *reliable and generic* predictions of the rate and extent of distribution into the brainECF, especially for P-gp substrates. The aim of the current study is to determine whether in vitro data extracted from literature can be repurposed as input in a CNS-PBPK model to confidently predict rat brainECF PK for multiple P-gp substrates. Specifically, we want to establish how variability in transport data from different sources (for the same drug) influences prediction outcomes and model robustness. Importantly, we did not include any empirically derived scaling factors in the methodology, and instead we use a purely bottom-up approach for the prediction of brainECF PK.

Materials & methods

Structural overview of the developed CNS PBPK model (LeiCNS-PK3.4)

Predictions of rat brain ECF PK were made by building on the previously published LeiCNS-PK3.0 PBPK model, which is able to accurately predict unbound CNS PK in multiple CNS compartments in rats, mice and humans [32–34]. This model leverages drug physicochemical properties, physiological properties of the CNS, and systemic plasma PK to predict CNS disposition. All changes that we made in the model structure concerned the movement of drugs across the BBB into or out of the brainECF. Though disposition to the cerebral spinal fluid (CSF) is not evaluated in the current study, CSF compartments and distribution are still present in the model structure as previously described [32]. Though P-gp is also present at the blood-CSF-border (BCSFB) [35], this was not taken into consideration since the focus of the current study is on BBB transport.

Some changes were made to the LeiCNS-PK3.0 model to obtain the new LeiCNS-PK3.4 model (Fig. 1). First, in the LeiCNS-PK3.0 model, transcellular and paracellular diffusion across the BBB are modelled as separate processes. In our new model these are grouped together into a single CL term for passive diffusion ($CL_{passive}$). This is a step back, but in this case it was needed since the aim of the current study was to evaluate the reliability of in vitro derived data for predicting BBB disposition, and in reported in vitro data there is no distinction between paracellular and transcellular passive transport. Additionally, in this way the LeiCNS-PK3.4 model can be compared directly with previously published PBPK models that apply similar methods for passive diffusion across the BBB [20–23]. Then, as P-gp mediated clearance (CL_{Pgp}) is explicitly accounted for in LeiCNS-PK3.4, the asymmetry factor (AF) was not required in the current model (i.e., for P-gp substrates) since the AF accounts for processes that drive $Kp_{uu,brain}$ away from unity, which is mainly driven by P-gp efflux for P-gp substrates. Thus, LeiCNS-PK3.4 can be informed completely by in vitro derived information to describe drug distribution across the BBB.

Determining drug clearances across the BBB

All drug movement across the BBB in vivo was predicted by using parameters from transwell permeability assays, as schematically illustrated in Fig. 2. In short, a drug is dosed at either the apical (A) or basolateral (B) side of a monolayer transfected with P-gp. The rate of appearance in the other chamber is subsequently measured, from which the apparent permeability (P_{app}) of a drug from each side of the monolayer to the other can be determined [9, 10]. Coadministration of a P-gp inhibitor or using a cell line that is not transfected with P-gp allows for the measurement of permeability without P-gp mediated CL (P_{app}[I]). The efflux ratio (ER), which is the ratio of the basolateral to apical ($P_{app,B:A}$) and apical to basolateral ($P_{app,A:B}$) permeability, highlights the degree of efflux mediated by P-gp. To account for the effect of other transporters that might influence the disposition across the membrane, the ER can be divided by the ER obtained when P-gp is inhibited (ER[I]). By doing so, the corrected efflux ratio (ER_c) is calculated [10, 36], which represents the effect that solely P-gp has on asymmetric transport across the monolayer (see Fig. 2).

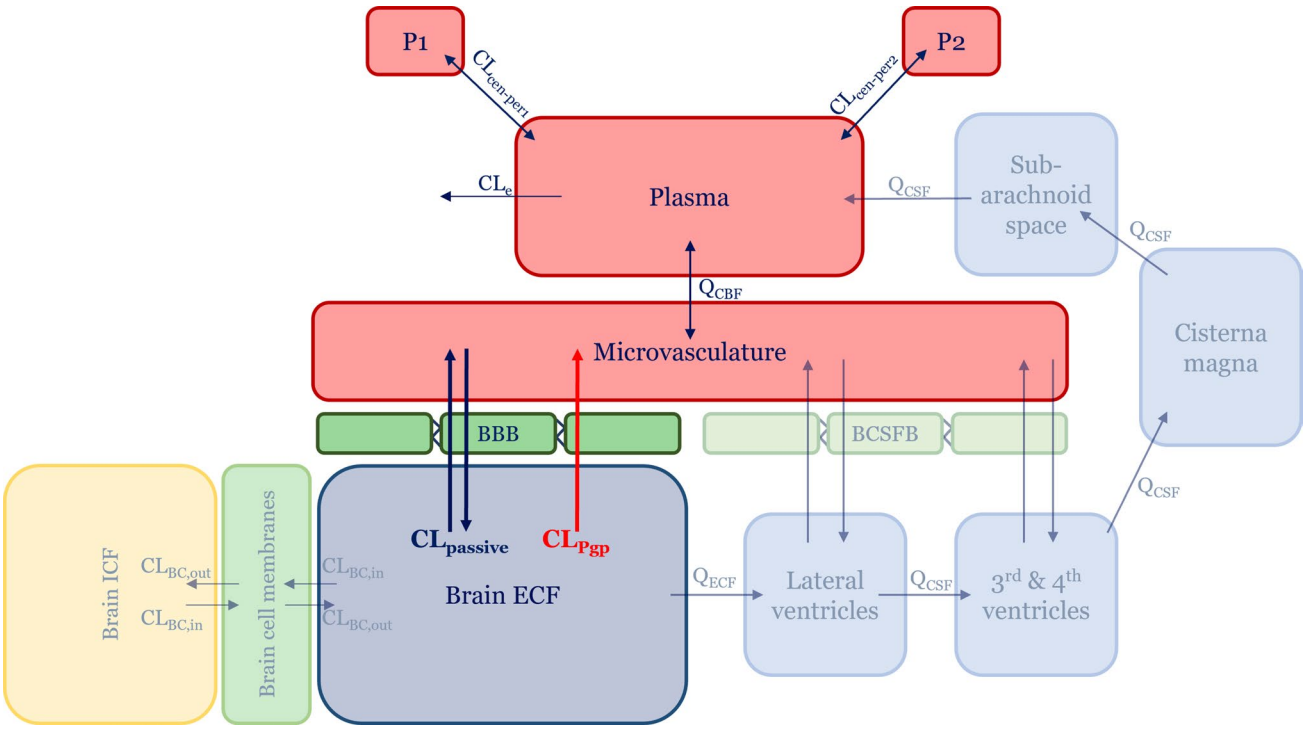

Fig. 1 Schematic of the LeiCNS-PK3.4 model structure. The LeiCNS model contains multiple CNS compartments, including intracellular fluid and cerebrospinal fluid compartments. The focus of the current study is on the distribution of drug from the brain microvasculature to the brain extracellular fluid across the blood–brain-border, through the passive clearance (blue bold arrows) and P-gp mediated clearance (CL_{Pgp}, red bold arrow). All aspects that are unchanged compared to LeiCNS-PK3.0 and that are not discussed in this study are shown with reduced opacity. *BBB* Blood–brain-border, *BCSFB* Blood-cerebrospinal fluid-border, $CL_{BC,in}$ Clearance into brain cell membranes, $CL_{BC,out}$ Clearance out of brain cell membranes, $CL_{cen\text{-}per1/2}$ Intercompartmental clearance, CL_e Systemic clearance, $CL_{passive}$ Passive clearance, CL_{Pgp} P-gp mediated clearance, *ECF* Extracellular fluid, *ICF* Intracellular fluid, *P1* Peripheral compartment 1, *P2* Peripheral compartment 2, Q_{CBF} cerebral blood flow, Q_{CSF} cerebral spinal fluid flow, Q_{ECF} ECF bulk flow (Color figure online)

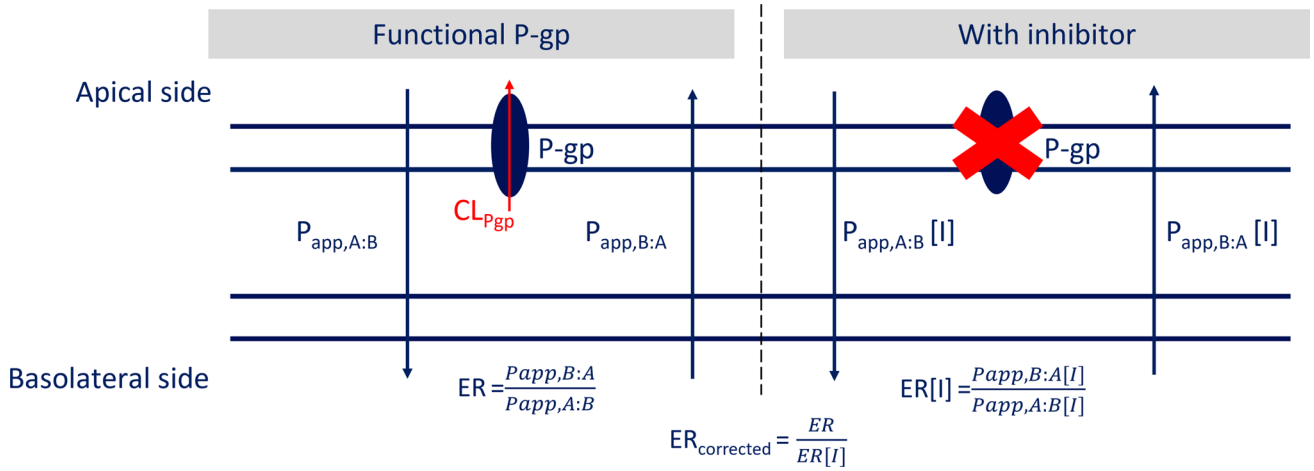

Fig. 2 Schematic overview of in vitro transwell assays and related membrane transport parameters. A drug is dosed at either the apical (**A**) or basolateral (**B**) side of a monolayer transfected with P-gp. The rate of appearance in the other chamber is subsequently measured, from which the apparent permeability (P_{app}) of a drug from one side of the monolayer to the other can be determined (displayed on the left). Coadministration of an inhibitor, or using a cell line that does not express P-gp, allows for measurements of P_{app} without P-gp (P_{app}[I]), which is displayed on the right

Passive diffusion of drugs across the BBB in vivo ($CL_{passive}$, Fig. 1) was calculated as [20–23]:

$$CL_{passive} = P_{app,A:B}[I] * SA_{BBB} * 60 \quad (1)$$

where $P_{app,A:B}$[I] is the apparent permeability ($\times 10^{-6}$ cm/s) from the apical to the basolateral direction with inhibition of P-gp (or derived from a cell line not transfected with P-gp) and SA_{BBB} is the surface area of the BBB in rats (155 cm^2 [32]). The expression was multiplied by 60 to express $CL_{passive}$ in mL/min. The P-gp mediated clearance (CL_{Pgp}) was determined through the method adapted from Kalvass et al. [37]:

$$CL_{Pgp} = (ER_c - 1) * 2P_{app,A:B}[I] * SA_{BBB,trans} * REF * 60 \quad (2)$$

where ER_c is the corrected efflux ratio in vitro (see Fig. 2) and $SA_{BBB,trans}$ is the surface area of the rat BBB available for transcellular processes ($SA_{BBB,trans} = 0.998 * SA_{BBB} = 154.69$ cm^2 [32]), since P-gp is embedded in the apical membrane of endothelial cells [38]. The multiplication by 60 is done to express CL_{Pgp} in mL/min.

Additionally, to account for differences in expression and activity of P-gp between in vitro and in vivo, we applied a proteomics-informed relative expression factor (REF) [15, 20, 39]:

$$REF = \frac{Pgp\ expression\ in\ vivo}{Pgp\ expression\ in\ vitro} \quad (3)$$

where the P-gp protein expression in vivo and in vitro is given in fmol/µg total protein. Of note is that use of the REF assumes the existence of a linear correlation between expression of P-gp and its activity [40, 41], and that its intrinsic activity (i.e., the activity of one entity of P-gp) is system-independent.

Equations (1) and (2) were subsequently introduced into LeiCNS-PK3.4. Changes in the amount of drug in the model compartments over time were described through ordinary differential equations. A change in unbound drug in the brainECF compartment of the final model was defined as:

$$V_{ECF}\frac{dC_{ECF}}{dt} = CL_{passive} * f_{up} * C_{MV} - \left(CL_{Pgp} + CL_{passive}\right) * C_{ECF} - Q_{ECF} * C_{ECF} - CL_{BC,in} * C_{ECF} * PHF_{ECF} + CL_{BC,out} * C_{BC} \quad (4)$$

where V_{ECF} is the volume of the brainECF and C_{MV}, C_{ECF}, and C_{BC} are drug concentrations in the brain microvasculature, brainECF, and brain cell membranes, respectively. f_{up} is the unbound fraction of drug in plasma, and Q_{ECF} is the bulk flow of brainECF to the lateral ventricles. $CL_{BC,in}$ and $CL_{BC,out}$ are clearances that describe drug partitioning into and out of brain cell membranes, and were calculated as described previously [32]. PHF_{ECF} is the fraction of drug that is unionized and available for partitioning into the brain cell membranes from the ECF [32]. All concentrations and clearances are expressed in ng/mL and mL/min, respectively.

In vivo microdialysis data for model evaluation

The developed model was evaluated using in vivo unbound brainECF PK profiles obtained through microdialysis in rats. Predictions of passive diffusion across the BBB were

evaluated using the plasma and brainECF PK data on the passively diffusing drugs acetaminophen, raclopride, and paliperidone (which is a P-gp substrate) co-administrated with tariquidar (a P-gp inhibitor). All in vivo data for the passively diffusing drugs were published previously and available in-house [42]. The prediction of P-gp functionality was evaluated with the P-gp substrates morphine, quinidine, risperidone, paliperidone (without tariquidar co-administration), and verapamil. A distinction was made between microdialysis data obtained from (ultra) short infusion of the drug (intravenous [I.V.] and subcutaneous [S.C.]) and data from a loading dose and maintenance constant rate infusion. The short infusion in vivo data were reported previously and available in-house for morphine [43], quinidine [44], and paliperidone [45]. For risperidone, data were extracted from literature [46]. The risperidone brainECF data were corrected for microdialysis lag time. Morphine plasma PK data concerned total plasma concentrations and were corrected for plasma protein binding in the model structure (f_{up} in Eq. (4)). Continuous infusion data were available for paliperidone, quinidine, risperidone and verapamil and were extracted from the study by Nagaya et al. [47]. An overview of the different drugs, doses, and references are shown in Table 1.

Overview of input parameters

Input parameters for the CNS PBPK model can be divided into four types: drug physicochemical parameters, physiological parameters, plasma pharmacokinetic parameters and drug transport parameters. Drug physicochemical properties and rat CNS physiological properties are listed in the Supplementary Tables 1 and 2. The plasma PK profile of a drug served as an input function for the model to predict distribution into the CNS and is described with an empirical population PK model. All PK models for the short infusion data were reported previously [32, 42, 46]. The risperidone PK parameters were adapted so that all parameters are expressed in millilitres and describe a typical rat weighing 0.25 kg. The continuous infusion plasma PK data were not described well using the previously reported PK models. As this is a prerequisite to evaluate the accuracy of the P-gp mediated CL, the PK models were re-estimated to fit a one compartment PK model using Monolix (version 2023R1, Lixoft, Antony, France) [49]. The PK parameters used to describe systemic plasma concentrations of the drugs are shown in Table 2.

The transport parameters of each drug (i.e., $P_{app,A:B}$, $P_{app,B:A}$, $P_{app,A:B}[I]$, $P_{app,B:A}[I]$, ER, and ER_c), and P-gp expression in vitro and in vivo were retrieved from previously published literature (Table 3). Values were retrieved from multiple sources using multiple cell lines, where possible, to assess the influence of different experimental conditions and variability in reported parameter values on model functionality.

Model evaluation

Model evaluation was done by calculating prediction errors (PEs) [20, 45] as:

$$PE = \frac{Y_{pred,j} - Y_{obs,i,j}}{(Y_{pred,j} + Y_{obs,i,j})/2}$$

where $Y_{pred,j}$ is the model predicted typical concentration at time point j and $Y_{obs,i,j}$ is the observed concentration for the *ith* individual at time point j. An optimal prediction would render a median PE of 0, but predictions were deemed accurate when the median PE fell within twofold error ($-0.67 \leq PE \leq 0.67$) compared to the observed data.

Table 1 Summary of the dosing regimens

	Drug	Administration route	Total dose (mg/kg body weight*)	Infusion time (minutes)	References
Short infusion	Acetaminophen	I.V	15	10	[48]
	Raclopride	I.V	0.56	10	[42]
	Morphine	I.V	40	10	[43]
	Paliperidone	I.V	0.5	20	[45]
	Quinidine	I.V	20	10	[44]
	Risperidone	S.C	3	N/A	[46]
Continuous infusion	Paliperidone	I.V	0.8 (L)/4 (M)	240	[47]
	Quinidine	I.V	8.0 (L)/20 (M)	240	[47]
	Risperidone	I.V	0.7 (L)/4 (M)	240	[47]
	Verapamil	I.V	0.9 (L)/4 (M)	240	[47]

I.V Intravenous, *S.C* subcutaneous, *N/A* not available for the dosage form, *(M)* maintenance dose, *(L)* loading dose. *Body weight of a typical rat was set to 0.25 kg in the predictions

Table 2 Pharmacokinetic parameters of the validation drugs in rats

	Drug	CL_{cen} (mL/min)	$Q_{cen\text{-}per1}$ (mL/min)	$Q_{cen\text{-}per2}$ (mL/min)	V_{cen} (mL)	V_{per1} (mL)	V_{per2} (mL)	K_a (1/min)
Short infusion	Acetaminophen (1)	4.7	11.2	31.4	50.7	27892	162.5	N/A
	Raclopride (1)	47.7	16.5	56.8	83	603	457.5	N/A
	Morphine (2)	22.6	30.8	7.2	152	530	1200	N/A
	Paliperidone (1)	219.5	6766	0	25	32,981	0	N/A
	Quinidine (1)	178.3	238	754	184	7335	5063	N/A
	Risperidone (3)	77	0	0	5250	0	0	0.03
Continuous infusion	Paliperidone (4)	29.2	0	0	2053	0	0	N/A
	Quinidine (4)	25	0	0	7314	0	0	N/A
	Risperidone (4)	37	0	0	3799	0	0	N/A
	Verapamil (4)	72.3	0	0	11,700	0	0	N/A

(1): From Saleh et al. (2021) [32]. (2) From Yamamoto et al (2017)42. (3): From Cremers et al. (2012) [46], recalculated for a rat weighing 0.25 kg. (4): Estimated

Software

Plasma PK parameters for the continuous infusion datasets were estimated using Monolix (version 2023R1, Lixoft, Antony, France) [49]. Literature data reported in plots was extracted using WebPlotDigitizer version 4.6 [64]. Development, execution of the LeiCNS-PK3.4 model and subsequent visualizations of the results were all done using RStudio version 4.3.0 [65]. The model was simulated using the freely available R package rxode2 version 2.0.13, while data visualization was done using the R package ggplot2.

Results

Reported apparent permeability of P-gp substrates in literature

In total, 34 sets of in vitro passive permeability ($P_{app,A:B}[I]$) and corrected efflux ratio (ER_c) for the drugs were retrieved from previously published literature. Cell lines used for the transport assays were Caco-2, MDCKII transfected with human P-gp (MDR1), and LLC-PK1 transfected with either rodent (mdr1a) or human (MDR1) P-gp. For the P-gp substrates, P_{app} values were available for quinidine and risperidone from all cell lines, while information on morphine, paliperidone and verapamil permeability was missing for either LLC-PK1 (morphine) or Caco-2 (paliperidone and verapamil).

In vitro transport values extracted from literature showed varying degrees of variability of $P_{app,A:B}[I]$ and ER_c for the P-gp substrates (Fig. 3 and Table 3). Similar $P_{app,A:B}[I]$ and ER_c between different sources and cell lines was observed for morphine (mean $P_{app,A:B}[I] \pm SD = 2.7 \pm 1.2 \times 10^{-6}$ cm/s, mean $ER_c \pm SD = 1.5 \pm 0.2$) and paliperidone (mean $P_{app,A:B}[I] \pm SD = 14.9 \pm 1.4 \times 10^{-6}$ cm/s, mean $ER_c \pm SD = 5.6 \pm 2.0$). However, the $P_{app,A:B}[I]$ of quinidine, risperidone and verapamil showed a higher degree of variability, with risperidone passive permeability ranging approximately 62-fold between sources. This variation was not distinctly related to a specific cell line, and large variability could be observed within a single cell line. For example, risperidone $P_{app,A:B}[I]$ values measured in LLC-PK1 cells ranged from 15.8×10^{-6} to 96.3×10^{-6} cm/s (mean ± SD of $41.6 \pm 33.8 \times 10^{-6}$ cm/s). For quinidine, $P_{app,A:B}[I]$ was similar for Caco-2 and LLC-PK1, except for the value reported by Nagaya et al. in LLC-PK1 cells (mean ± SD of $55.9 \pm 2.4 \times 10^{-6}$ cm/s without Nagaya et al. $P_{app,A:B}[I]$). Permeability of quinidine in MDCKII cells was lower than in Caco-2 and LLC-PK1 and also varied, with the values reported by Bicker et al. and Feng et al. aligning with a mean of 8.76×10^{-6} cm/s, whereas the $P_{app,A:B}[I]$ from Troutman et al. was higher (36.8×10^{-6} cm/s).

Though the risperidone and verapamil $P_{app,A:B}[I]$ values vary substantially, the ER_c values were more consistent between sources, except for the ER_c reported by Uchida et al. which were higher than the other values for both drugs. Like the $P_{app,A:B}[I]$, the quinidine ER_c showed great variability (mean $ER_c \pm SD = 10.4 \pm 9.0$), with the reported ER_c varying up to 22-fold between Caco-2 and LLC-PK1-mdr1a based studies.

P-gp expression is constant in vivo but variable in vitro

In vivo P-gp expression in rat brain microvascular endothelial cells was constant between different sources, with a mean of 19.4 fmol/μg total protein (see Supplementary Table 3). In contrast, in vitro expression of P-gp in the cell lines showed a high degree of variability (see Supplementary

Table 3 Apparent passive permeability $P_{app,A:B}[I]$ and corrected efflux ratio (ER_c) of P-gp substrates derived from literature

Drug	Cell line	$P_{app,A:B}[I]$ ($\times 10^{-6}$ cm/s)	ER_c	References
Acetaminophen	Caco-2	31.9*	1	Kamiya et al. (2020) [50]
Raclopride	Caco-2	73.4 [Zosquidar, KO-143, Benzbromarone]	1.1†	Colclough et al. (2024) [51]
Morphine	Caco-2	2.08 [Cyclosporine A]	1.6	Crowe (2002)[52]
	MDCKII-MDR1	2.12	1.3	Verscheijden et al. (2021) [20]
	MDCKII-MDR1	1.8	1.3	Feng et al. (2008) [53]
	MDCKII-MDR1	4.8	1.9	Garberg et al. (2005) [54]
Paliperidone	LLC-PK1-mdr1a	14.7	8.1	Inoue et al. (2012) [55]
	LLC-PK1-MDR1	13.3	5.3	Inoue et al. (2012) [55]
	MDCKII-MDR1	16.8	3.3	Feng et al. (2008) [53]
Quinidine	Caco-2	52.0 [GF120918]	4.3	Korjamo et al. (2006) [56]
	Caco-2	58.9 [Verapamil]	1.5	Mukkavilli et al. (2017) [57]
	Caco-2	54.5 [GW918]	5.2	Troutman & Thakker (2003a) [58]
	LLC-PK1-mdr1a	56.90	16.1	Nicolaï et al. (2020) [16]
	LLC-PK1-mdr1a	57.2	32.8	Uchida et al. (2011) [15]
	LLC-PK1-MDR1	15.9	12.9	Nagaya et al. (2020) [59]
	MDCKII-MDR1	9.52	5.9	Bicker et al. (2017) [60]
	MDCKII-MDR1	8.0	7.4	Feng et al. (2008) [53]
	MDCKII-MDR1	36.8	7.3	Troutman & Thakker (2003b) [61]
Risperidone	Caco-2	1.56 [Verapamil]	4.1	Cousein et al. (2007) [62]
	LLC-PK1-mdr1a	15.8	3.6	Inoue et al. (2012) [55]
	LLC-PK1-mdr1a	66.2	2.1	Nicolaï et al. (2020) [16]
	LLC-PK1-mdr1a	96.3	10.6	Uchida et al. (2011) [15]
	LLC-PK1-MDR1	14.0	3.4	Inoue et al. (2012) [55]
	LLC-PK1-MDR1	15.6	3.9	Nagaya et al. (2014) [63]
	MDCKII-MDR1	19.8	2.0	Feng et al. (2008) [53]
	MDCKII-MDR1	53.6 [GF120918]	1.7	Mahar Doan et al. (2002) [9]
Verapamil	LLC-PK1-mdr1a	41.5	2.9	Nicolaï et al. (2020) [16]
	LLC-PK1-mdr1a	73.5	13.3	Uchida et al. (2011) [15]
	LLC-PK1-MDR1	22.3	5.4	Nagaya et al. (2014) [63]
	LLC-PK1-MDR1	47.1	2.7	Nicolaï et al. (2020) [16]
	MDCKII-MDR1	12.6	2.1	Feng et al. (2008) [53]
	MDCKII-MDR1	44.0 [GF120918]	1.74	Mahar Doan et al. (2002) [9]
	MDCKII-MDR1	28.6	2.65	Troutman & Thakker (2003b) [61]
	MDCKII-MDR1	30.0	3.10	Garberg et al. (2005) [54]

For $P_{app,A:B}[I]$, the P-gp inhibitor used to measure passive diffusion is given in square brackets. When no inhibitor is specified, $P_{app,A:B}[I]$ was determined in parental cell lines. *Assumed $P_{app,A:B}[I]$ to be the same as $P_{app,A:B}$ without inhibitor due to not being transported by P-gp. † Efflux ratio determined in MDCKI-MDR1 cell line

Table 3). Table 4 shows the highest and lowest reported P-gp protein expression in each cell line, as well as the average of these values. Only one P-gp expression level was reported for the LLC-PK1-MDR1 cell line, and this was categorized under the lowest expression due to its proximity to the lowest value of the LLC-PK1-mdr1a cell line. This is however an arbitrary distinction.

BrainECF PK is predicted well for passively diffusing drugs

Predictions of brainECF PK were first evaluated for drugs undergoing passive diffusion, to ensure adequate model functionality before including CL_{Pgp}. BrainECF PK was predicted for three drugs that diffuse passively across the BBB, namely acetaminophen, raclopride and, in case of P-gp inhibition by tariquidar, paliperidone

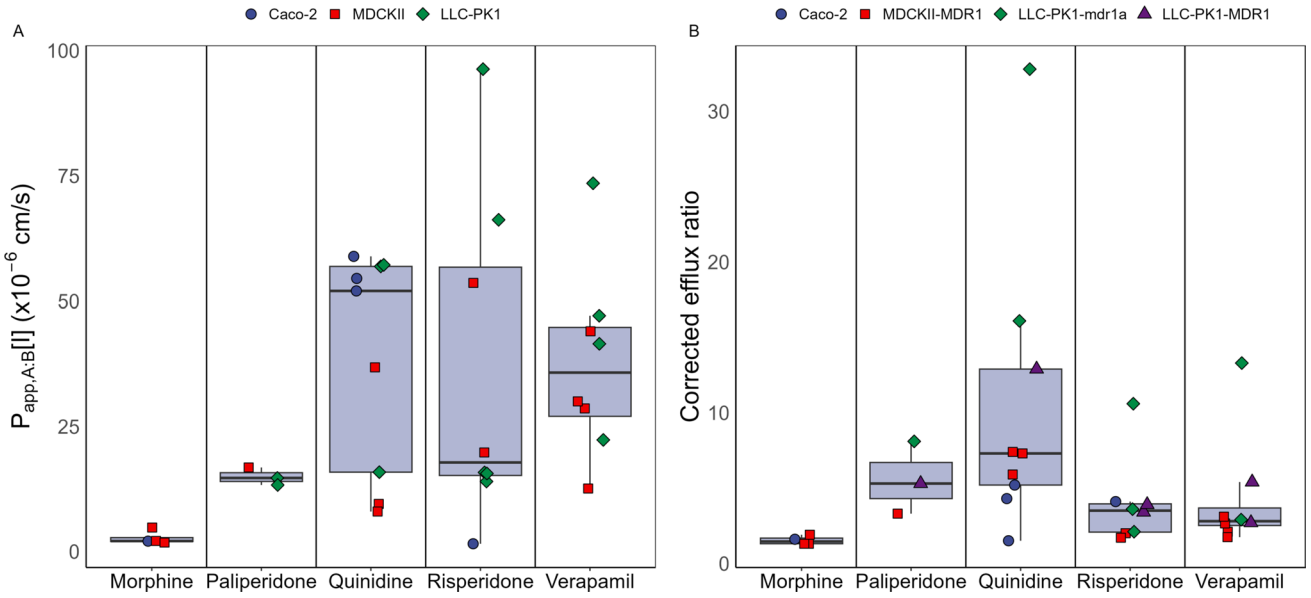

Fig. 3 Overview of **A** $P_{app,A:B}[I]$ and **B** corrected efflux ratio (ER_c) per drug. Different cell lines are indicated by shapes and colours of the observed datapoints (Color figure online)

Table 4 Expression of P-gp in different cell lines in vitro

Cell line	Highest P-gp expression (fmol/µg protein)	Average P-gp expression (fmol/µg protein)*	Lowest P-gp expression (fmol/µg protein)
Caco-2	7.4[$]	4.7	2
LLC-PK1-MDR1	–	–	13.1
LLC-PK1-mdr1a	61	38.1	15.2
MDCKII-MDR1	10.3	6.3	2.2[#]

Due to variability in the reported values, the expression values are categorized into the highest, lowest, and average reported expression levels. All P-gp expression levels and references are given in Supplementary Table 3 *Average of highest and lowest expression values. [$]Mean of the P-gp expressions reported by Harwood et al. (2016) [66] and Miliotis et al. (2011) [67]. [#]Mean of the P-gp expressions reported by Di et al. (2011) [68], Feng et al. (2019) [69], and Jacqueroux et al. (2020) [70]

(Fig. 4). Plasma PK data of these drugs were described well by the plasma PK model, and the LeiCNS-PK3.4 model adequately predicted the observed brainECF PK profiles within a two-fold median prediction error (PE). The raclopride prediction did slightly underestimate the time to maximum concentration (T_{max}) observed in the brainECF.

Brain ECF PK prediction accuracy varies between P-gp substrates and dosing schemes

Predictions of rat brainECF PK were made for five P-gp substrates (Fig. 5). Observed plasma PK data (Supplementary Fig. 1) were described accurately within twofold PE. To account for the reported variability in P-gp expression in vitro, predictions of P-gp substrates' brainECF PK were made using the lowest, average, and highest P-gp expression levels reported for each cell line (Table 4). The resulting brainECF predictions are represented through a prediction interval, with the upper and lower bounds of the coloured bands in Fig. 5 corresponding to the predictions made with the highest and lowest in vitro P-gp expression, respectively. The predictions for the average in vitro P-gp expression are shown as a black line. As such, each transport value has three predictions associated to it, except for the LLC-PK1-MDR1 based predictions, since only one in vitro expression value was reported for this cell line.

After administration of a short infusion (or subcutaneous dose), the morphine and risperidone brainECF predictions were accurate across the different transport values and expression levels (Fig. 5A). An overview of the percentage of the predictions that fall within twofold prediction error (PE) per in vitro expression level is shown in Table 5. The PEs for every single prediction (i.e., predictions of each

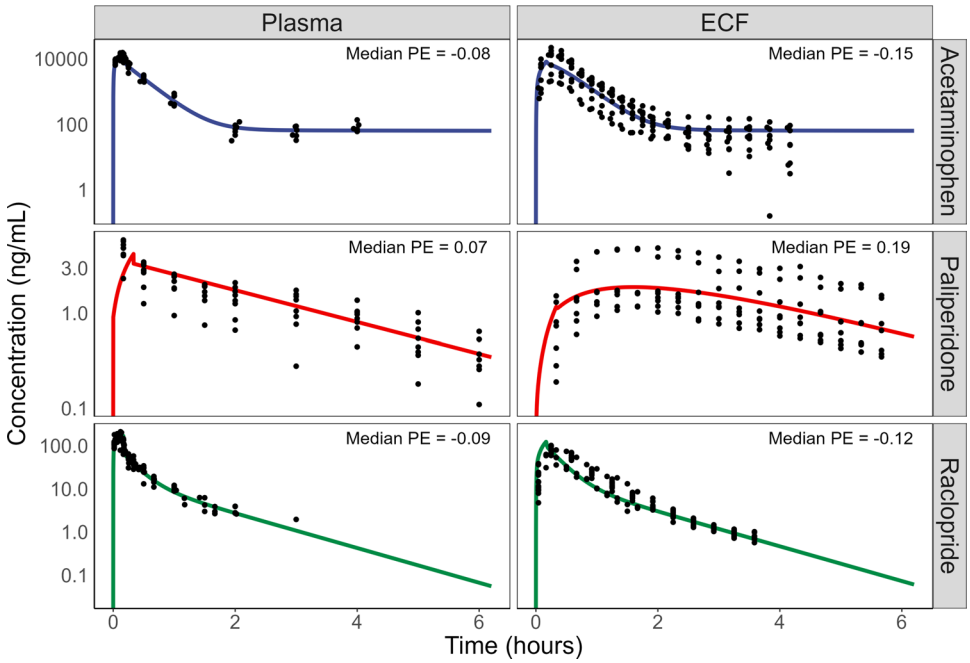

Fig. 4 Description of unbound plasma PK and prediction of rat brainECF PK of the passively diffusing drugs acetaminophen, paliperidone co-administered with the P-gp inhibitor tariquidar, and raclopride. These predictions serve as a validation of whether the model is able to accurately predict brain distribution in the absence of P-gp mediated transport. Median PE (calculated as outlined in methods Sect. "Model evaluation") is shown in the top-right of each subfigure. For the paliperidone prediction, the $P_{app,A:B}[I]$ value of 14.7 * 10^{-6} cm/s from Inoue et al. was used

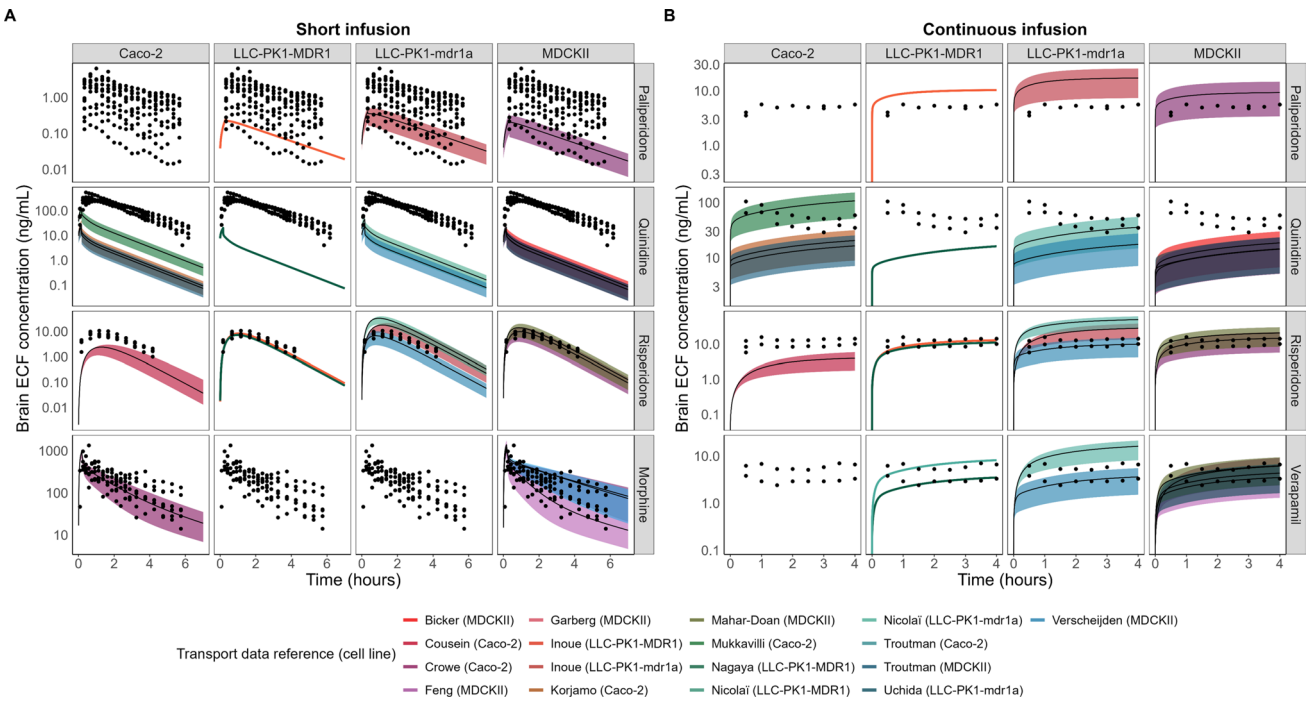

Fig. 5 Rat brainECF PK predictions after **A** short infusion (or subcutaneous dose administration) and **B** continuous infusion after loading dose of the P-gp substrates paliperidone, quinidine, risperidone, morphine and verapamil. Each column shows which cell line was used to determine $P_{app}[I]$ and ER_c values that were used as input for the prediction. The colour of the prediction interval corresponds to the colours given below the table, which specifies the reference from which transport data were retrieved (shown in Table 3). The upper line of the prediction bands indicates the predictions made using the highest in vitro P-gp expression value for the given cell line, while the lowest line of the band corresponds to the lowest expression value. Black lines indicate the prediction made using the average in vitro P-gp expression. Each row indicates a different drug. Plots without predictions indicate lack of transport data in a cell line for a given drug. Observed unbound brainECF concentrations are shown as black points

Table 5 Percentage of all predictions that fall within twofold median prediction error (PE) for each drug per in vitro expression value used to inform the REF

	% of predictions within 2-fold PE per *in vitro* P-gp expression level (number of predictions / total amount of predictions)			
	Highest	Average	Lowest	No REF
Morphine				
Short infusion	50 (2/4)	100 (4/4)	50 (2/4)	50 (2/4)
Continuous infusion	-	-	-	-
Paliperidone				
Short infusion	0 (0/2)	0 (0/2)	0 (0/3)	0 (0/3)
Continuous infusion	0 (0/2)	50 (1/2)	100 (3/3)	33.3 (1/3)
Quinidine				
Short infusion	0 (0/8)	0 (0/8)	0 (0/9)	0 (0/9)
Continuous infusion	37.5 (3/8)	25.0 (2/8)	11.1 (1/9)	55.6 (5/9)
Risperidone				
Short infusion	50 (3/6)	66.7 (4/6)	62.5 (5/8)	50 (4/8)
Continuous infusion	33.3 (2/6)	66.7 (4/6)	62.5 (5/8)	50 (4/8)
Verapamil				
Short infusion	-	-	-	-
Continuous infusion	83.3 (5/6)	83.3 (5/6)	37.5 (3/8)	62.5 (5/8)

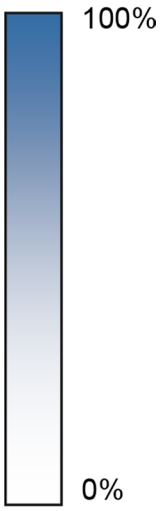

The prediction accuracy for each drug for both the short infusion data (Fig. 5A) and the continuous infusion data (Fig. 5B) is shown. Aside from the in vitro expression levels, the model accuracy when not using a REF is shown ("No REF" column). The number of predictions that are successful compared to the total amount of predictions for a given drug at a certain in vitro expression level are given in brackets behind the percentage. Darker blue cells indicate that more predictions fall within twofold PE, while lighter cells correspond to fewer successful predictions

individual reference and per expression level) are shown in Supplementary Tables 4 and 5. Table 5 also shows the accuracy of predictions that were made without the REF (predictions shown in Supplementary Fig. 2). All the morphine brainECF predictions fell within twofold median PE using the average in vitro P-gp expression value (Table 5). The risperidone brainECF predictions showed the best performance with the average or low P-gp expression, with only one of the references being unable to accurately predict the observed brainECF data with any of the P-gp expression values (Cousein et al., using Caco-2 cells, supplementary Table 4). None of the paliperidone or quinidine short infusion predictions fell within twofold PE (Table 5), with the quinidine predictions reaching ± 100-fold underprediction (Supplementary Table 4).

For the continuous infusion data (Fig. 5B), the observed verapamil brainECF PK was predicted well, with almost all the predictions falling within twofold median PE using either the highest or average in vitro P-gp expression. The brainECF PK predictions for a continuous infusion of risperidone showed similar trends as observed for the predictions after subcutaneous administration (compare Fig. 5A and B). The paliperidone brainECF predictions during the continuous infusion tend to slightly overpredict the observed data but showed < twofold PE with the low in vitro expression value in each cell line (Table 5). Overall, the continuous infusion quinidine data tended to be underpredicted, with 37.5% of the predictions falling within twofold using the high P-gp expression.

Assessment of prediction accuracy based on different stratifications of the input

Next, we assessed the accuracy of the model predictions when stratifying on different factors. Taking all predictions together (i.e., regardless of cell line or in vitro expression level), the model accurately predicted brainECF PK profiles within twofold median PE for 2 of the 4 short infusion drug dosing regimens and 3 of the 4 drugs for the continuous infusions (Fig. 6A). Across all cell lines, the LLC-PK1-MDR1, LLC-PK1-mdr1a and MDCKII cell lines showed similar prediction accuracies for the different drugs (Fig. 6B). The MDCKII cell lines however showed a higher degree of overlap between predictions than the LLC-PK1-mdr1a cells (Fig. 5).

Lastly, the brainECF prediction accuracies were investigated per cell line and expression level for each drug (Fig. 7). It shows that there is not one clear in vitro expression value that is the most accurate for predictions, which can also be concluded from the results in Table 5. Instead, to what extent P-gp activity has to be modulated appears to be drug dependent, as can for example be seen for the continuous infusion predictions obtained using data from the LLC-PK1-mdr1a cell line as input. Here, paliperidone and risperidone required the lowest in vitro expression value, verapamil the average value, and quinidine the highest in vitro expression value. In theory, the REF value used for scaling should depend on the experimental condition only and not on the drug. A few studies reported transport

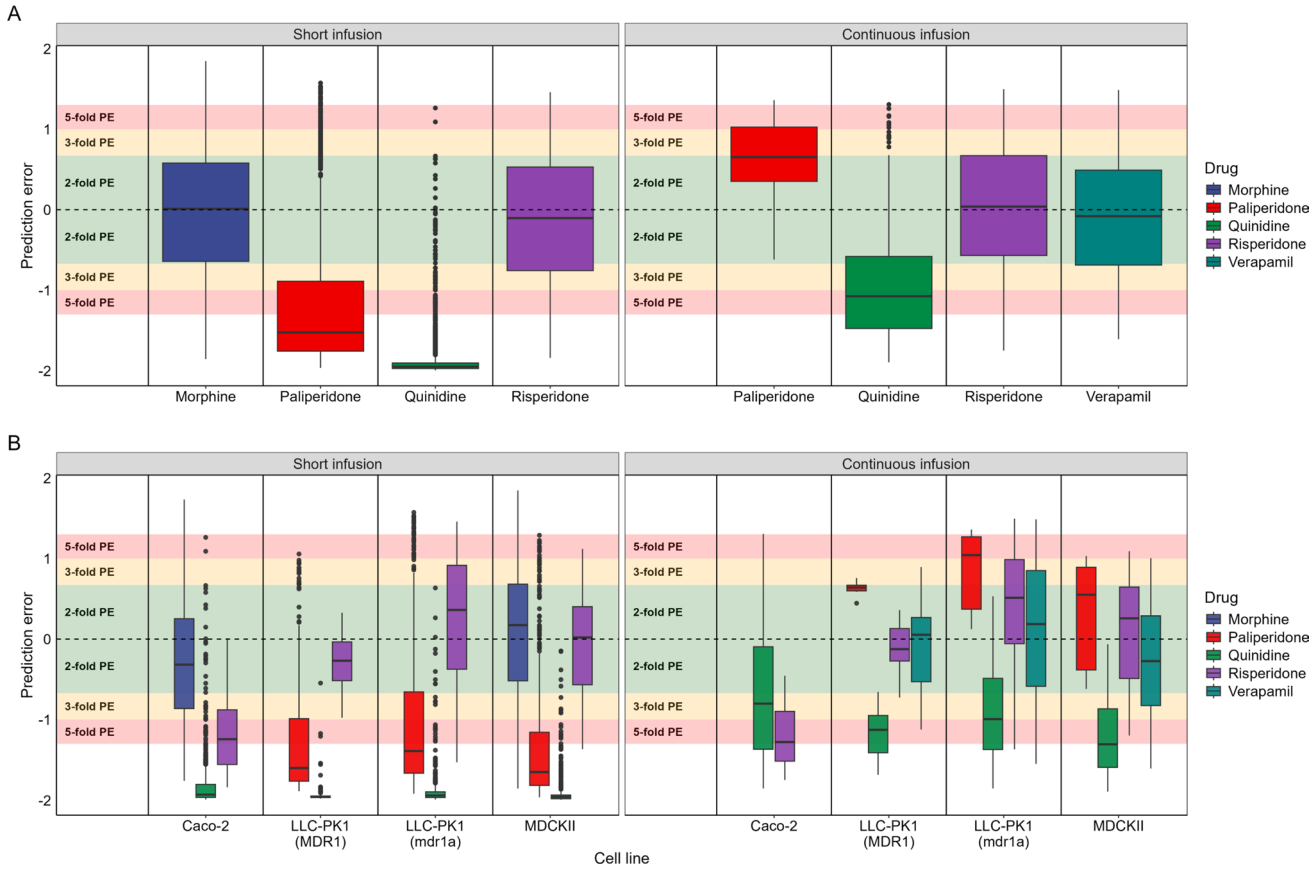

Fig. 6 Prediction errors (PE) of the short infusion (left panel) and the continuous infusion with loading dose (right panel) datasets. **A** Overall prediction errors per drug by considering all of the predictions regardless of cell line or in vitro expression level used as input. **B** Prediction errors of the model per drug stratified by the in vitro cell lines. All expression levels (highest, average, and lowest) are considered. Colours of the boxes correspond to the drug in both subplots (**A**) and (**B**). The areas corresponding to < 2-, < 3- and < fivefold over- and underprediction are highlighted in green, yellow and red, respectively. The PE of 0 is indicated by a dashed line. Black dots show outliers that fall outside of the minimum or maximum boxplot range (Color figure online)

values for multiple drugs (i.e., values were obtained under the same experimental condition), and plotting the prediction errors of the continuous infusion data per drug showed that a single scaling factor (e.g., low expression) results in different prediction accuracies between the drugs, even when transport values were derived from the same experimental setup (Supplementary Fig. 3).

Using in vitro expression and permeability data from the same experiment does not guarantee an accurate brainECF prediction

The risperidone, quinidine and verapamil permeability data extracted from Uchida et al. and Nicolaï et al. were reported in conjunction with the expression of P-gp in the studied cell line (lowest and highest expression in LLC-PK1-mdr1a cells, respectively). Combining the expression and transport data from the same experimental system should, in theory, give the best predictions. Whenever the transport values and P-gp expression data were correctly matched, almost all predictions were more than three-fold over or underpredicted, whereas using the incorrect in vitro expression value (i.e., the expression reported by the other reference) gave better (within twofold PE) predictions (Table 6). For the LLC-PK1-MDR1 based prediction of verapamil, matching the transport values reported by Nicolaï et al. to the P-gp expression reported for LLC-PK1-MDR1 cells in the same article (13.1 fmol/µg) did give an accurate prediction (median PE = 0.28).

Variability in in vitro derived parameters impacts the predicted rate and extent of distribution to the brain

To appreciate the impact of the variability in $P_{app.A:B}[I]$ and ER_c on the predicted rates and extent of drug distribution, we simulated the subcutaneous administration of risperidone and short infusion of morphine over a range

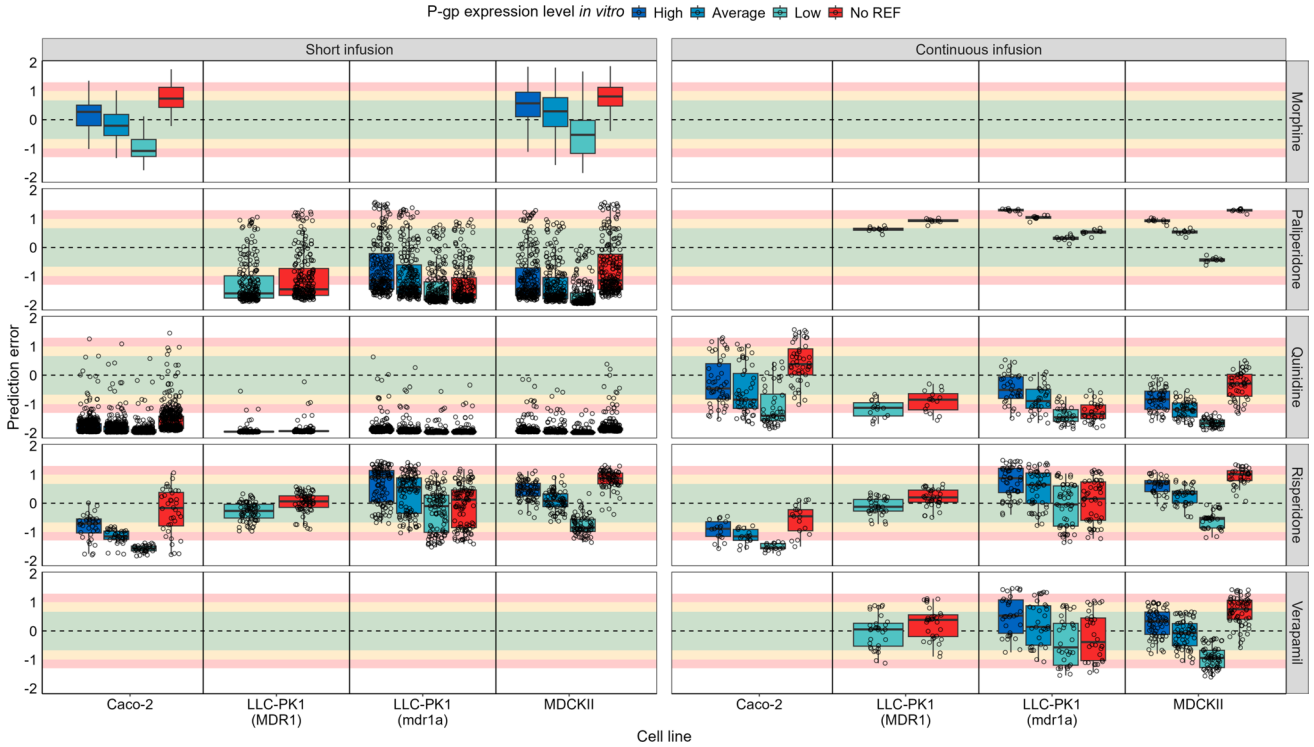

Fig. 7 Prediction errors of the model brainECF PK predictions for each drug (rows), stratified by the cell line used in-vitro to determine transport parameters (columns) and the in-vitro P-gp expression used for the scaling of CL_{Pgp} from in vitro to in vivo (box colour). In addition to the predictions made using the three in vitro expression values, the predictions made without considering the REF are shown (red boxplots). The areas corresponding to < 2-, < 3- and < fivefold over- or underprediction are highlighted in green, yellow, and red, respectively. The PE of 0 is indicated with a dashed line. To enhance the clarity of the figure, individual points for morphine were omitted (Color figure online)

Table 6 Median prediction errors of risperidone, quinidine and verapamil predictions made using LLC-PK1-mdr1a transport data from Uchida et al. [15] and Nicolaï et al. [16], using the LLC-PK1-mdr1a in vitro P-gp expression reported by Uchida et al. and by Nicolaï et al. PE values shaded in green, yellow and red fall within twofold error, threefold error and > threefold error, respectively

	Risperidone (Subcutaneous)		Risperidone (Constant infusion)		Quinidine (Constant infusion)		Verapamil (Constant infusion)	
	Uchida transport data	Nicolaï transport data	Uchida transport data	Nicolaï transport data	Uchida transport data	Nicolaï transport data	Uchida transport data	Nicolaï transport data
Uchida expression	-1.14	0.56	-1.08	0.65	-1.56	-1.18	-1.2	0.28
Nicolaï expression	-0.04	1.23	0.06	1.25	-0.71	-0.05	-0.1	1.09

of input values (Fig. 8). The LeiCNS-PK3.4 simulations are shown as continuous lines. The predicted profile that is obtained by only scaling the plasma PK profile by the observed $Kp_{uu,BBB}$ (extent of distribution) is shown as a dashed, red line. For risperidone, the scaled plasma profile shows a good match with the extent of risperidone distribution, but overpredicts the rate of distribution (Fig. 8A). The morphine prediction using only the $Kp_{uu,BBB}$ to scale

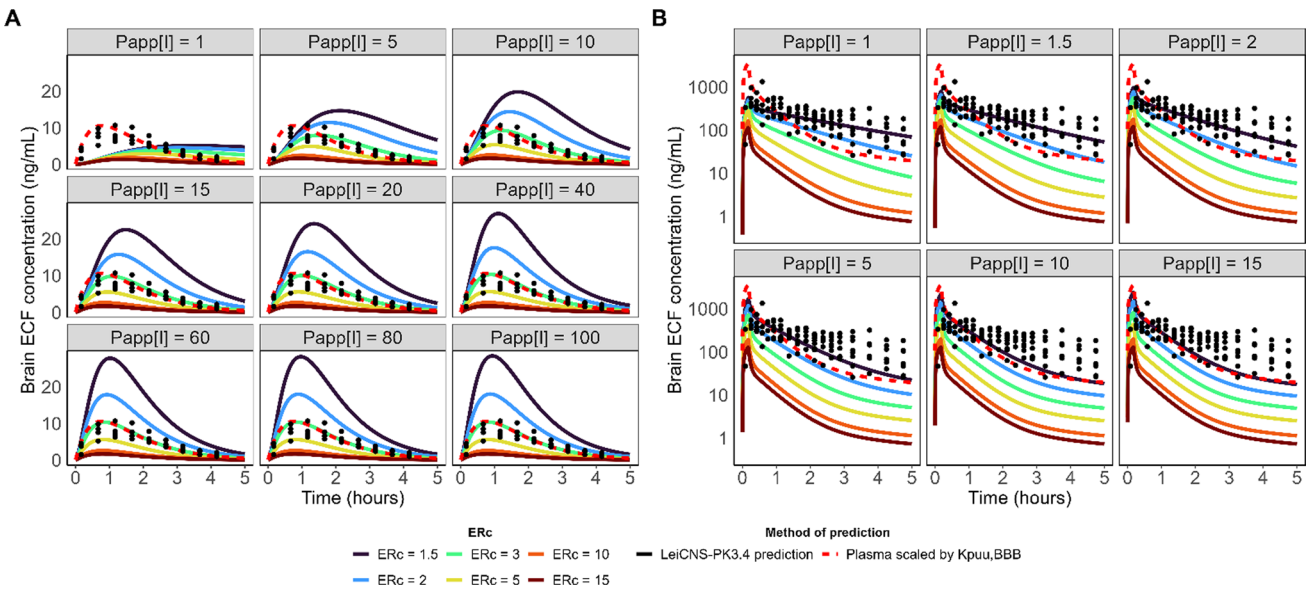

Fig. 8 Impact of varying passive permeability ($P_{app}[I]$) and ER_c on the predicted brainECF PK profiles of risperidone and morphine. The passive permeability used as input into the LeiCNS-PK3.4 model is given in the headers, while the ER_c used as input is indicated by the colour of the line. **A** Risperidone simulations are given using in vitro P-gp expression of 13.1 fmol/µg protein as reported in LLC-PK1-MDR1 cells. The dashed red line represents the unbound plasma concentration profile scaled by the observed $Kp_{uu,BBB}$ of 0.147 (i.e., $C_{ECF} = C_{plasma,u} * Kp_{uu,BBB}$). **B** Morphine simulations are given using the average in vitro P-gp expression in Caco-2 cells of 4.7 fmol/µg protein. The dashed red line represents the unbound plasma concentration profile scaled by the observed $Kp_{uu,BBB}$ of 0.23. For both subplots, $P_{app}[I]$ values are given in 10^{-6} cm/s. Black dots are observed microdialysis data. The LeiCNS-PK3.4 simulations are shown as continuous lines. $P_{app}[I]$ here represents $P_{app,A:B}[I]$ (Color figure online)

the plasma profile misrepresents the observed rate of distribution in the brain ECF (Fig. 8B). The LeiCNS-PK3.4 simulations highlight that increasing passive permeability shifts the predicted rates of distribution to follow the shape of the plasma profile more closely. Variability in the ER_c mostly impacts the predicted extent of distribution. However, especially for risperidone at lower ($< 20 * 10^{-6}$ cm/s) passive diffusion speed, increasing ER_c also impacts the predicted T_{max} (Fig. 8A). The impact of variability in passive permeability on the predicted rate of distribution for passively diffusing compounds shows similar behaviour, with high diffusion speeds approaching the shape of the plasma profile (Supplementary Fig. 4).

Discussion

Transport data (e.g., $P_{app}[I]$ and ER_c) for many drugs are widely available in literature, and have shown promise for prediction of P-gp mediated drug distribution across the BBB. An important distinction should be made here between predicting extent of distribution (i.e., the ratio of unbound drug concentration between brain ECF and plasma at steady state, $Kp_{uu,BBB}$) and rate (i.e., with what speed a drug crosses the BBB) [17]. PBPK models allow for prediction of temporal profiles (representing both rate and extent) based on in vitro information, without relying on in vivo studies. However, in vitro data are known to be variable, the impact of which had not yet been investigated for CNS PBPK modelling. Additionally, the suitability of this data for brainECF PK predictions of multiple drugs and dosing schemes is not yet fully characterized. We therefore evaluated the reliability of literature derived in vitro data for in vivo predictions of brainECF PK, by introducing an in vitro informed P-gp mediated clearance into the LeiCNS-PBPK model (LeiCNS-PK3.4).

In vitro transport data are informative of the in vivo rate of passive distribution

The LeiCNS-PK3.4 model was able to accurately predict unbound brainECF PK in the absence of active processes. This is in agreement with previous CNS PBPK models, which showed the same description of passive diffusion ($CL_{passive}$) to allow accurate predictions of CSF distribution of passively diffusing compounds [19, 71, 72]. The $P_{app,A:B}[I]$ reported in literature for the passively diffusing compounds were either only available from one source or did not vary greatly. Simulations of the passively diffusing drugs (Supplementary Fig. 4) however show that varying passive diffusion has a great impact on the predicted rate of distribution of the drugs. The fact that we were able to adequately predict the brainECF PK of these compounds using

the currently applied values therefore show the translational value of the in vitro transport data to in vivo.

Nicolaï et al. had to reduce in vitro passive diffusion tenfold for accurate prediction of $Kp_{uu,brain}$ [16]. Such a reduction in passive diffusion rate has great implications for the predictions of temporal PK, as shown by the risperidone simulations. The risperidone passive permeability reported by Cousein et al. for example was more than tenfold lower than other risperidone transport values [62], which resulted in a poor prediction of the rate of distribution (Fig. 5). This highlights the difference between prediction of $Kp_{uu,brain}$ (extent) and temporal brain (ECF) PK profiles (both rate and extent). Accurate prediction of one does not guarantee an accurate prediction of the other. This was also shown by Storelli et al., who predicted $Kp_{uu,brain}$ using in vitro data within twofold of the observed value, but subsequently underpredicted temporal PK profiles [73].

In the risperidone and morphine simulations (Fig. 8) we included a prediction based on scaling the plasma profile by the extent of distribution ($Kp_{uu,BBB}$). This resulted in a predicted rate of distribution that did not follow the observed rate of distribution, which was especially clear for a slowly diffusing compound like morphine. This shows the importance of separately accounting for rate and extent when predicting CNS exposure. The simulations show that the interplay between $P_{app,A:B}[I]$ and ER_c is important in determining the final temporal PK profiles.

Variability in vitro impacts the predicted rate and extent of drug distribution and therefore reliability of the model

Including P-gp mediated clearance (CL_{Pgp}) based on literature-derived in vitro data showed promising predictions for most of the P-gp substrates. The values of in vitro-derived parameters are different between sources, which can lead to markedly different predicted extents of distribution for the P-gp substrates, most clearly seen for the continuous infusion dosing regimens (Fig. 5B) (see for example the LLC-PK1-mdr1a based risperidone predictions). The MDCKII-MDR1 derived transport data, which show a high degree of variability in $P_{app,A:B}[I]$ for quinidine, risperidone and verapamil, showed the least variability in ER_c of the different cell lines, leading to the most similar predicted extents of distribution between sources. The model simulations support the observation that variability in ER_c is the major factor in determining the predicted extent of distribution.

$P_{app,A:B}[I]$ was also found to be variable between sources, which has important implications for the predicted rate of distribution to the brain (Fig. 8, Supplementary Fig. 4). Our risperidone simulations show that $P_{app,A:B}[I]$ values higher than 20×10^{-6} cm/s mirror the shape of the plasma PK profile, rather than the observed rate of distribution in the brain ECF. The two LLC-PK1-mdr1a based risperidone predictions using the data from Uchida et al. and Nicolaï et al. ($P_{app,A:B}[I] = 96.3 \times 10^{-6}$ cm/s and 66.2×10^{-6} cm/s, respectively) therefore overpredict the rate of distribution as observed in vivo. The in vitro data by Nagaya et al., Inoue et al. and Feng et al. seem to resemble risperidone's PK in vivo more closely. The reason for why exactly these studies report such different values for $P_{app,A:B}[I]$ should be studied more thoroughly, in order to serve as a robust input for LeiCNS-PK3.4.

The morphine simulations (Fig. 8B) indicate a requirement of low $P_{app.A:B}[I]$ and low ER_c in order to accurately capture both rate and extent of distribution in vivo. This agrees with what is reported in vitro for morphine, allowing accurate predictions of morphine's rate and extent of distribution by LeiCNS-PK3.4. This shows that in vitro data can indeed hold important mechanistic information on a P-gp substrate's distribution behaviour in vivo. We observe however that the variability observed for both $P_{app,A:B}[I]$ and ER_c has substantial impact on the robustness of the predicted rates and extent, which should be kept in mind when using in vitro data, especially when it is derived from a single source and not compared to other articles.

Accounting for P-gp expression in vitro

Most of the published transport data did not report $P_{app,A:B}[I]$ and ER_c in conjunction with in vitro P-gp expression. The P-gp expression in vitro was found to be highly variable in literature. Therefore, instead of using a single P-gp expression value, we made predictions for the bandwidth of reported P-gp expression values. From that we conclude that the REF greatly influences the extent of drug distribution, and thereby the prediction accuracy. This is in line with Fenneteau et al. who identified the scaling factor associated with P-gp expression to be a sensitive parameter in their PBPK model [74], as well as the results by Ball et al. who showed an important role of the REF (named RAF in their study) on the predicted brainECF profile [23]. Most of the transport data have a median PE within twofold error when combined with one or multiple of the reported P-gp expression levels (Table 5 and Supplementary Tables 4 and 5). This indicates that currently, as long as the underlying reasons for variability in P-gp expression data are unknown and the actual P-gp expression in vitro is not given, this bandwidth P-gp expression approach gives a good indication of the PK profile in vivo.

Uncertainty in in vitro P-gp expression and its effect on the prediction of intestinal permeability has been investigated by Harwood et al., who recommended that both expression and permeability should be measured in

conjunction for accurate IVIVE [75]. This was echoed by Verscheijden et al. who had to estimate a scaling factor in their brain PBPK model, since a REF based on a literature-derived expression value did not adequately describe observed data [19]. Interestingly, for the cases in which we combined LLC-PK1-mdr1a transport values with in vitro P-gp expression that were reported in conjunction, we observed poor prediction accuracies (> threefold PE, Table 6). In fact, for LLC-PK1-mdr1a, using in vitro expression values reported by other studies gave better predictions for risperidone, quinidine and verapamil than using the in vitro expression level given in the same publication (Table 6). We will now discuss multiple ideas that might (partly) explain this observation.

Are P-gp expression and its activity linearly related?

Uchida et al. consistently reported a higher ER_c than Nicolaï et al., even though Nicolaï et al. reported an in vitro P-gp expression 4-fold higher than Uchida et al. [15, 16]. Based on the assumed correlation between expression of P-gp and its functionality, we would expect the P-gp expression to also be lower for Nicolaï et al. This is also what the model indicates to be required for accurate predictions (Table 6). When Nicolaï et al. scaled only through a REF, they observed a poor prediction accuracy of the $Kp_{uu,brain}$ which they tended to overpredict (our predictions using Nicolaï data similarly overpredict the observed data, Table 6) [16]. A tenfold reduction of passive permeability allowed for more accurate predictions in their study. Not considered by Nicolaï et al. (nor by our model) is the distinction between *total* P-gp and *efflux active* (or functional) P-gp in a cell line [76, 77]. Functional P-gp is expressed at or near the tips of microvilli, which can successfully expel a drug [76]. Drug expelled by P-gp at the sides of microvilli ('inactive' P-gp) however will promptly collide with the membranes of neighbouring villi and be reabsorbed. The amount of functional P-gp has been reported to be tenfold lower than the total amount of P-gp in Caco-2 cells [76]. LLC-PK1 cells also possess microvilli [78, 79], as such a discrepancy between total P-gp and functional P-gp might explain why the Nicolaï et al. data require lower in vitro expression levels in our model predictions. It does not explain why the Uchida et al. efflux ratios are so high, as the functional P-gp concentration would have to be higher than the total amount to justify the use of a higher expression level than reported.

Besides the distinction between total and active P-gp, we might also question our and others' assumptions (1) that activity and expression of P-gp are linearly correlated, and (2) that this relationship is drug-independent. A linear relationship between expression and activity of P-gp in vitro has been reported for quinidine, verapamil and vinblastine [40, 41]. This has also been reported for BCRP and OATP1B1 when normalizing to Na^+-K^+ ATPase expression [80]. In vivo, changes in intestinal P-gp expression influenced uptake of P-gp substrates [81]. However, others were unable to correlate expression and functionality of P-gp. A study on the hCMEC/D3 BBB cell line showed that an increase in both mRNA and protein expression of P-gp did not influence transport of rhodamine-123, a strong P-gp substrate [82]. Similarly, Kosztyu et al. were not able to relate P-gp expression (either protein or mRNA) to its activity in vitro [83]. Expression of P-gp on lymphocytes also did not show a relationship to functionality [84, 85], and an in vivo study showed that changes in P-gp protein expression at the rat BBB did not influence quinidine efflux [86]. At the dog BBB, individual differences in P-gp and BCRP expression did not correlate with the $K_{p,brain}$ of quinidine and apafant (P-gp substrates) or dantrolene and daidzein (BCRP substrates) [87].

In the linear correlations reported by Tachibana et al., a change in expression did not yield the same change in maximum P-gp activity (V_{max}) for different drugs [40]. Sanchez-Dengra et al. developed a PBPK model to predict brainECF PK, and fit empirical scaling factors for their IVIVE approach. They obtained different estimates depending on the drug, and correlated the scaling factors in a non-linear fashion with logP [88]. A drug-dependency of the scaling factor can also be observed in the current study. We first observed that a single scaling factor as applied in the current methodology is not generically applicable across drugs (Table 5 and Fig. 7). Moreover, a comparison of the PEs of the continuous infusion predictions made using the low in vitro P-gp expression for references that reported transport values for multiple drugs, showed a trend of $PE_{paliperidone} > PE_{risperidone} > PE_{verapamil} > PE_{quinidine}$ (supplementary Fig. 3). If differences in P-gp activity between in vitro and in vivo would only depend on P-gp expression, a single scaling factor should give similar prediction errors for data retrieved from a single experimental setup. Overall, the current results are in line with other reports which suggest that the relationship between expression and activity of P-gp is not straightforward, at least at the BBB. Considering drug-specific differences together with differences in P-gp expression and morphology of the cell line(s) might therefore prove important for successful and robust IVIVE of CL_{Pgp} at the BBB.

Methodological considerations

To account for the effect of other (endogenous) transporters present in vitro, we made use of the corrected efflux ratio (ER_c). This was done by dividing the ER (obtained in the P-gp expressing cell line) by the ER[I], which is obtained though chemical inhibition of P-gp or by measuring in the parental cell line that does not overexpress P-gp. Chemical

inhibitors that were used in the in vitro studies are Cyclosporine A, GF120918, verapamil and GW918. Cyclosporine A, GF120918 and verapamil all also inhibit BCRP and MRP1 [89]. Parental cell lines also are not perfect copies of the transfected cell line, as transporter expression might differ [90]. As such, it is likely that the currently calculated ER_c does not purely represent P-gp activity if a drug is a substrate for multiple transporters. For future research, it is recommend to investigate whether using a P-gp specific inhibitor [91] to determine ER[I] might be more reliable for a description of purely P-gp.

Another aspect that might improve the method is to use pmol transporter per gram (pmol/g) wet tissue weight as a measure of expression, instead of fmol P-gp/µg total protein [15, 39, 92]. This unit reduces inter-laboratory variability in transporter expression, as it accounts for differences in sample preparations and purity of the determined protein amounts [93]. An approach to convert fmol/µg protein to pmol/g wet tissue has been proposed [94, 95], however, this requires substantial knowledge of the experimental setup, which is not easily extracted from literature. Additionally, in vitro P-gp expression has not yet been reported in this unit, which restricted the current study to use of fmol/µg.

We did not limit the in vitro studies to those that use the rat homologue of P-gp, but also included mouse and human derived P-gp. We did not think this would significantly influence the rat brainECF PK predictions, as the rat, mouse and human homologues of P-gp share a highly conserved amino acid sequence (sequence similarity of 92% mouse-human, 97% mouse-rat) [96]. Additionally, others previously reported similar binding characteristics on a molecular level [96], a good correlation in mouse and rat ER in vitro [97], similar functionality in vivo of rat and mouse P-gp [98], and a good correlation between human and mouse P-gp ER ($R^2 = 0.92$, $n = 3300$) [53]. Moreover, our model predictions do not show an inability of one of the homologues to accurately predict rat brainECF PK.

Quinidine influx and differences between short infusion and continuous infusion dosing

The final point we would like to discuss is the difference between the short infusion (S.I.) and continuous infusion (C.I.) data of quinidine. The S.I. quinidine data was reported by Westerhout et al. [44]. P-gp was functional in this study, as coadministration of the P-gp inhibitor tariquidar significantly increased the $Kp_{uu,brain}$ from 1.5 to 8.6. Therefore, these results indicate significant P-gp activity but also a role for influx transport of quinidine in vivo (as $Kp_{uu,brain} > 1$) that is not (sufficiently) present in vitro. This is supported by other reports that have indicated quinidine to be influxed by an influx transporter (like OATP1 or OATP2) and/or to inhibit influx of other compounds [99–102]. Ishida et al. have reported quinidine to be influxed during in vitro experiments in the Caco-2 cell line [103]. Quinidine is an example of how our model can highlight important physiological aspects in vivo that might be missed in vitro. Of note is that the influx led to great underprediction of the S.I. data (± 100-fold), but not of the C.I. data (overall underprediction between ± threefold and ± sixfold), giving predictions within threefold PE for all transport data when using the high in vitro expression. The extent of drug distribution varies between different brain regions [104]. This might play a role as the C.I. dataset measured ECF data in the hippocampus and frontal cortex, while the S.I. dataset measured in the striatum. The difference in rat type might also play a role as the C.I. dataset used Sprague–Dawley rats [47] while the S.I. dosing used Wistar rats [44]. Finally, the difference in the administration itself (C.I. versus S.I.) might influence the BBB transport kinetics. Overall, the reason for the difference in the C.I. and S.I. quinidine (and also paliperidone) datasets is unclear and warrants further investigation. Estimation of the influx together with P-gp transport [21] might allow for these aspects to be computationally studied.

Conclusions

This study highlights that accurate rat brainECF PK predictions of passively diffusing drugs and P-gp substrates are possible by informing a PBPK model with in vitro data obtained from literature. Especially predictions based on data from MDCKII-MDR1 cells showed a high degree of agreement in the predicted extent of distribution between different studies, due to little variation in reported ER_c of drugs. In general, variability in ER_c strongly affects predicted extents of distribution. Variability in $P_{app,A:B}[I]$ was substantial (also within cell lines), which has important implications for the predicted rate of distribution. Large variability in the reported in vitro P-gp expression influenced robustness of the model predictions and confidence in the predictions when using a single value. Instead, bandwidth predictions based on the extremes of reported in vitro P-gp expression allowed a brainECF PK prediction area, giving a good indication about what to expect in vivo. However, whenever transport data and in vitro P-gp expression reported by a single study were used as input together, this did not guarantee an accurate prediction. Scaling in vitro CL_{Pgp} to in vivo only through differences in P-gp expression might as such not completely capture the differences in functionality. Important mechanistic information about the relationship between P-gp expression and functionality appears to be missing for robust scaling of P-gp activity at the BBB. Looking

beyond just expression differences and considering other (drug-specific) factors might therefore improve the robustness of the IVIVE approach.

Supplementary Information The online version contains supplementary material available at https://doi.org/10.1007/s10928-025-09963-w.

Author contributions DWvV, ECMdL, and MH conceptualized the study; DWvV performed the computational work, analysis and wrote the main manuscript text; DWvV, VR and ECMdL interpreted the results; ECMdL and VR supervised the project; DWvV, ECMdL, VR, and MH reviewed and edited the manuscript.

Funding This project has received funding from the European Union's Horizon 2020 research and innovation programme under Grant Agreement No 848068. This article reflects only the authors' view and the European Commission is not responsible for any use that may be made of the information it contains.

Data availability All data supporting the results in this study can be found within the main text and Supplementary Materials.

Declarations

Conflict of interest M.H. is an employee of Daiichi-Sankyo Co., Ltd. The other authors declare no conflicts of interest.

References

1. Wong AD et al (2013) The blood-brain barrier: an engineering perspective. Front Neuroeng 6:7
2. Kesselheim AS, Hwang TJ, Franklin JM (2015) Two decades of new drug development for central nervous system disorders. Nat Rev Drug Discov 14(12):815–816
3. Kaitin KI, DiMasi JA (2011) Pharmaceutical innovation in the 21st century: new drug approvals in the first decade, 2000–2009. Clin Pharmacol Ther 89(2):183–188
4. Schinkel AH (1999) P-Glycoprotein, a gatekeeper in the blood-brain barrier. Adv Drug Deliv Rev 36(2–3):179–194
5. Clay AT, Sharom FJ (2014) Multidrug resistance protein: P-glycoprotein. In: Guofeng YM, Morris M (eds) Drug transporters. Wiley, Hoboken
6. de Lange EC, Hammarlund-Udenaes M (2015) Translational aspects of blood-brain barrier transport and central nervous system effects of drugs: from discovery to patients. Clin Pharmacol Ther 97(4):380–394
7. de Lange EC et al (2005) Toward the prediction of CNS drug-effect profiles in physiological and pathological conditions using microdialysis and mechanism-based pharmacokinetic-pharmacodynamic modeling. AAPS J 7(3):E532–E543
8. Bagchi S et al (2019) In-vitro blood-brain barrier models for drug screening and permeation studies: an overview. Drug Des Dev Ther 13:3591–3605
9. Mahar Doan KM et al (2002) Passive permeability and P-glycoprotein-mediated efflux differentiate central nervous system (CNS) and non-CNS marketed drugs. J Pharmacol Exp Ther 303(3):1029–1037
10. Schwab D et al (2003) Comparison of in vitro P-glycoprotein screening assays: recommendations for their use in drug discovery. J Med Chem 46(9):1716–1725
11. Storelli F et al (2022) The next frontier in ADME science: predicting transporter-based drug disposition, tissue concentrations and drug-drug interactions in humans. Pharmacol Ther 238:108271
12. Loryan I et al (2022) Unbound brain-to-plasma partition coefficient, K(p, uu, brain)-a game changing parameter for CNS drug discovery and development. Pharm Res 39(7):1321–1341
13. Summerfield SG et al (2006) Improving the in vitro prediction of in vivo central nervous system penetration: integrating permeability, P-glycoprotein efflux, and free fractions in blood and brain. J Pharmacol Exp Ther 316(3):1282–1290
14. Langthaler K et al (2024) Application of a new MDCKII-MDR1 cell model to measure the extent of drug distribution in vitro at equilibrium for prediction of in vivo unbound brain-to-plasma drug distribution. Fluids Barriers CNS 21(1):11
15. Uchida Y et al (2011) Blood-brain barrier (BBB) pharmacoproteomics: reconstruction of in vivo brain distribution of 11 P-glycoprotein substrates based on the BBB transporter protein concentration, in vitro intrinsic transport activity, and unbound fraction in plasma and brain in mice. J Pharmacol Exp Ther 339(2):579–588
16. Nicolaï J et al (2020) Impact of in vitro passive permeability in a P-gp-transfected LLC-PK1 model on the prediction of the rat and human unbound brain-to-plasma concentration ratio. Pharm Res 37(9):175
17. Hammarlund-Udenaes M et al (2008) On the rate and extent of drug delivery to the brain. Pharm Res 25(8):1737–1750
18. Murata Y et al (2022) In vitro to in vivo extrapolation linked to physiologically based pharmacokinetic models for assessing the brain drug disposition. AAPS J 24(1):28
19. Verscheijden LFM et al (2021) Differences in P-glycoprotein activity in human and rodent blood-brain barrier assessed by mechanistic modelling. Arch Toxicol 95(9):3015–3029
20. Verscheijden LFM et al (2021) Physiologically based pharmacokinetic/pharmacodynamic model for the prediction of morphine brain disposition and analgesia in adults and children. PLoS Comput Biol 17(3):e1008786
21. Li J et al (2017) Quantitative and mechanistic understanding of AZD1775 penetration across human blood-brain barrier in glioblastoma patients using an IVIVE-PBPK modeling approach. Clin Cancer Res 23(24):7454–7466
22. Badhan RK, Chenel M, Penny JI (2014) Development of a physiologically-based pharmacokinetic model of the rat central nervous system. Pharmaceutics 6(1):97–136
23. Ball K et al (2012) Development of a physiologically based pharmacokinetic model for the rat central nervous system and determination of an in vitro-in vivo scaling methodology for the blood-brain barrier permeability of two transporter substrates, morphine and oxycodone. J Pharm Sci 101(11):4277–4292
24. Gaohua L et al (2016) Development of a permeability-limited model of the human brain and cerebrospinal fluid (CSF) to integrate known physiological and biological knowledge: estimating time varying CSF drug concentrations and their variability using in vitro data. Drug Metab Pharmacokinet 31(3):224–233

25. Li J et al (2021) Physiologically based pharmacokinetic modeling of central nervous system pharmacokinetics of CDK4/6 inhibitors to guide selection of drug and dosing regimen for brain cancer treatment. Clin Pharmacol Ther 109(2):494–506
26. Fenneteau F et al (2009) Assessing drug distribution in tissues expressing P-glycoprotein through physiologically based pharmacokinetic modeling: model structure and parameters determination. Theor Biol Med Model 6:2
27. Dijkers M (2019) Reduce, reuse, recycle: good stewardship of research data. Spinal Cord 57(3):165–166
28. Volpe DA (2008) Variability in Caco-2 and MDCK cell-based intestinal permeability assays. J Pharm Sci 97(2):712–725
29. Harwood MD et al (2023) Interlaboratory variability in the Madin-Darby canine kidney cell proteome. Mol Pharm 20(7):3505–3518
30. Punt A et al (2023) Impact of in vitro experimental variation in kinetic parameters on physiologically based kinetic (PBK) model simulations. Altex 40(2):237–247
31. Lee JB et al (2017) Quantitative analysis of lab-to-lab variability in Caco-2 permeability assays. Eur J Pharm Biopharm 114:38–42
32. Saleh MAA et al (2021) Lumbar cerebrospinal fluid-to-brain extracellular fluid surrogacy is context-specific: insights from LeiCNS-PK3.0 simulations. J Pharmacokinet Pharmacodyn 48(5):725–741
33. Saleh MAA et al (2023) Using the LeiCNS-PK3.0 physiologically-based pharmacokinetic model to predict brain extracellular fluid pharmacokinetics in mice. Pharm Res. https://doi.org/10.1007/s11095-023-03554-5
34. Yamamoto Y et al (2018) Prediction of human CNS pharmacokinetics using a physiologically-based pharmacokinetic modeling approach. Eur J Pharm Sci 112:168–179
35. Morris ME, Rodriguez-Cruz V, Felmlee MA (2017) SLC and ABC transporters: expression, localization, and species differences at the blood-brain and the blood-cerebrospinal fluid barriers. AAPS J 19(5):1317–1331
36. Hu HH et al (2014) Evaluation of blood-brain barrier and blood-cerebrospinal fluid barrier permeability of 2-phenoxyindan-1-one derivatives using in vitro cell models. Int J Pharm 460(1–2):101–107
37. Kalvass JC, Pollack GM (2007) Kinetic considerations for the quantitative assessment of efflux activity and inhibition: implications for understanding and predicting the effects of efflux inhibition. Pharm Res 24(2):265–276
38. Sharom FJ (2014) Complex interplay between the P-glycoprotein multidrug efflux pump and the membrane: its role in modulating protein function. Front Oncol 4:41
39. Balhara A, Yin M, Unadkat JD (2023) Successful prediction of fetal exposure to dual BCRP/P-gp drug substrates using the efflux ratio-relative expression factor approach and PBPK M&S. Clin Pharmacol Ther. https://doi.org/10.1016/j.dmpk.2023.100809
40. Tachibana T et al (2010) Model analysis of the concentration-dependent permeability of P-gp substrates. Pharm Res 27(3):442–446
41. Shirasaka Y, Sakane T, Yamashita S (2008) Effect of P-glycoprotein expression levels on the concentration-dependent permeability of drugs to the cell membrane. J Pharm Sci 97(1):553–565
42. Yamamoto Y et al (2017) Predicting drug concentration-time profiles in multiple CNS compartments using a comprehensive physiologically-based pharmacokinetic model. CPT Pharmacomet Syst Pharmacol 6(11):765–777
43. Groenendaal D et al (2007) Population pharmacokinetic modelling of non-linear brain distribution of morphine: influence of active saturable influx and P-glycoprotein mediated efflux. Br J Pharmacol 151(5):701–712
44. Westerhout J et al (2013) The impact of P-gp functionality on non-steady state relationships between CSF and brain extracellular fluid. J Pharmacokinet Pharmacodyn 40(3):327–342
45. Yamamoto Y et al (2017) A generic multi-compartmental CNS distribution model structure for 9 drugs allows prediction of human brain target site concentrations. Pharm Res 34(2):333–351
46. Cremers TI et al (2012) Microdialysis evaluation of clozapine and N-desmethylclozapine pharmacokinetics in rat brain. Drug Metab Dispos 40(10):1909–1916
47. Nagaya Y et al (2016) Investigation of utility of cerebrospinal fluid drug concentration as a surrogate for interstitial fluid concentration using microdialysis coupled with cisternal cerebrospinal fluid sampling in wild-type and Mdr1a(-/-) rats. Drug Metab Pharmacokinet 31(1):57–66
48. Westerhout J et al (2012) Physiologically based pharmacokinetic modeling to investigate regional brain distribution kinetics in rats. AAPS J 14(3):543–553
49. *Monolix*. Lixoft SAS, a Simulations Plus company
50. Kamiya Y et al (2020) Determination and prediction of permeability across intestinal epithelial cell monolayer of a diverse range of industrial chemicals/drugs for estimation of oral absorption as a putative marker of hepatotoxicity. Toxicol Rep 7:149–154
51. Colclough N et al (2024) Utilizing a dual human transporter MDCKII-MDR1-BCRP cell line to assess efflux at the blood brain barrier. Drug Metab Dispos 52(2):95–105
52. Crowe A (2002) The influence of P-glycoprotein on morphine transport in Caco-2 cells comparison with paclitaxel. Eur J Pharmacol 440(1):7–16
53. Feng B et al (2008) In vitro P-glycoprotein assays to predict the in vivo interactions of P-glycoprotein with drugs in the central nervous system. Drug Metab Dispos 36:268–275
54. Garberg P et al (2005) In vitro models for the blood–brain barrier. Toxicol In Vitro 19(3):299–334
55. Inoue T et al (2012) Blonanserin, a novel atypical antipsychotic agent not actively transported as substrate by P-glycoprotein. Prog Neuropsychopharmacol Biol Psychiatry 39(1):156–162
56. Korjamo T et al (2006) Metabolic and efflux properties of Caco-2 cells stably transfected with nuclear receptors. Pharm Res 23(9):1991–2001
57. Mukkavilli R, Jadhav G, Vangala S (2017) Evaluation of drug transport in MDCKII-Wild Type, MDCKII-MDR1, MDCKII-BCRP and Caco-2 cell lines. Curr Pharm Biotechnol 18(14):1151–1158
58. Troutman MD, Thakker DR (2003) Efflux ratio cannot assess P-glycoprotein-mediated attenuation of absorptive transport: asymmetric effect of P-glycoprotein on absorptive and secretory transport across Caco-2 cell monolayers. Pharm Res 20(8):1200–1209
59. Nagaya Y et al (2020) Impact of P-glycoprotein-mediated active efflux on drug distribution into lumbar cerebrospinal fluid in nonhuman primates. Drug Metab Dispos 48(11):1183–1190
60. Bicker J et al (2017) Elucidation of the impact of P-glycoprotein and breast cancer resistance protein on the brain distribution of catechol-O-methyltransferase inhibitors. Drug Metab Dispos 45(12):1282–1291
61. Troutman MD, Thakker DR (2003) Novel experimental parameters to quantify the modulation of absorptive and secretory transport of compounds by P-glycoprotein in cell culture models of intestinal epithelium. Pharm Res 20(8):1210–1224
62. Cousein E et al (2007) P-glycoprotein and cytochrome P450 3A4 involvement in risperidone transport using an in vitro Caco-2/TC7 model and an in vivo model. Prog Neuropsychopharmacol Biol Psychiatry 31(4):878–886
63. Nagaya Y et al (2014) Utility of cerebrospinal fluid drug concentration as a surrogate for unbound brain concentration in nonhuman primates. Drug Metab Pharmacokinet 29(5):419–426

64. Rohatgi A (2022) *WebPlotDigitizer*
65. team, P., *RStudio: integrated development environment for R*. 2023, Posit Software, PBC
66. Harwood MD et al (2016) In vitro-in vivo extrapolation scaling factors for intestinal P-glycoprotein and breast cancer resistance protein: part I: a cross-laboratory comparison of transporter-protein abundances and relative expression factors in human intestine and Caco-2 cells. Drug Metab Dispos 44(3):297–307
67. Miliotis T et al (2011) Development of a highly sensitive method using liquid chromatography-multiple reaction monitoring to quantify membrane P-glycoprotein in biological matrices and relationship to transport function. Drug Metab Dispos 39(12):2440–2449
68. Di L et al (2011) Development of a new permeability assay using low-efflux MDCKII cells. J Pharm Sci 100(11):4974–4985
69. Feng B et al (2019) Validation of human MDR1-MDCK and BCRP-MDCK cell lines to improve the prediction of brain penetration. J Pharm Sci 108(7):2476–2483
70. Jacqueroux E et al (2020) Value of quantifying ABC transporters by mass spectrometry and impact on in vitro-to-in vivo prediction of transporter-mediated drug-drug interactions of rivaroxaban. Eur J Pharm Biopharm 148:27–37
71. Verscheijden LFM et al (2019) Development of a physiologically-based pharmacokinetic pediatric brain model for prediction of cerebrospinal fluid drug concentrations and the influence of meningitis. PLoS Comput Biol 15(6):e1007117
72. Bowman C et al (2023) Evaluation of bottom-up modeling of the blood-brain barrier to improve brain penetration prediction via physiologically based pharmacokinetic modeling. Biopharm Drug Dispos 44(1):60–70
73. Storelli F, Anoshchenko O, Unadkat JD (2021) Successful prediction of human steady-state unbound brain-to-plasma concentration ratio of P-gp substrates using the proteomics-informed relative expression factor approach. Clin Pharmacol Ther 110(2):432–442
74. Fenneteau F, Li J, Nekka F (2009) Assessing drug distribution in tissues expressing P-glycoprotein using physiologically based pharmacokinetic modeling: identification of important model parameters through global sensitivity analysis. J Pharmacokinet Pharmacodyn 36(6):495–522
75. Harwood MD et al (2016) In vitro-in vivo extrapolation scaling factors for intestinal P-glycoprotein and breast cancer resistance protein: part II. The impact of cross-laboratory variations of intestinal transporter relative expression factors on predicted drug disposition. Drug Metab Dispos 44(3):476–80
76. Bentz J, Ellens H (2021) Case study 8: status of the structural mass action kinetic model of P-gp-mediated transport through confluent cell monolayers. Methods Mol Biol 2342:737–763
77. Tran TT et al (2005) The elementary mass action rate constants of P-gp transport for a confluent monolayer of MDCKII-hMDR1 cells. Biophys J 88(1):715–738
78. Nielsen R et al (1998) Characterization of a kidney proximal tubule cell line, LLC-PK1, expressing endocytotic active megalin. J Am Soc Nephrol 9(10):1767–1776
79. Pfaller W, Gstraunthaler G, Loidl P (1990) Morphology of the differentiation and maturation of LLC-PK1 epithelia. J Cell Physiol 142(2):247–254
80. Kumar V et al (2015) Quantitative transporter proteomics by liquid chromatography with tandem mass spectrometry: addressing methodologic issues of plasma membrane isolation and expression-activity relationship. Drug Metab Dispos 43(2):284–288
81. Hoffmeyer S et al (2000) Functional polymorphisms of the human multidrug-resistance gene: multiple sequence variations and correlation of one allele with P-glycoprotein expression and activity in vivo. Proc Natl Acad Sci USA 97(7):3473–3478
82. Poller B et al (2010) Regulation of BCRP (ABCG2) and P-glycoprotein (ABCB1) by cytokines in a model of the human blood-brain barrier. Cell Mol Neurobiol 30(1):63–70
83. Kosztyu P et al (2015) Can the assessment of ABCB1 gene expression predict its function in vitro? Eur J Haematol 95(2):150–159
84. Vasquez EM et al (2005) An assessment of P-glycoprotein expression and activity in peripheral blood lymphocytes of transplant candidates. Transplant Proc 37(1):175–177
85. Vilas-Boas V et al (2011) P-glycoprotein activity in human Caucasian male lymphocytes does not follow its increased expression during aging. Cytometry A 79(11):912–919
86. De Lange ECM et al (2018) P-glycoprotein protein expression versus functionality at the blood-brain barrier using immunohistochemistry, microdialysis and mathematical modeling. Eur J Pharm Sci 124:61–70
87. Braun C et al (2017) Quantification of transporter and receptor proteins in dog brain capillaries and choroid plexus: relevance for the distribution in brain and CSF of selected BCRP and P-gp substrates. Mol Pharm 14(10):3436–3447
88. Sanchez-Dengra B et al (2021) Physiologically based pharmacokinetic (PBPK) modeling for predicting brain levels of drug in rat. Pharmaceutics 13(9):1402
89. Matsson P et al (2009) Identification of novel specific and general inhibitors of the three major human ATP-binding cassette transporters P-gp, BCRP and MRP2 among registered drugs. Pharm Res 26(8):1816–1831
90. Kuteykin-Teplyakov K et al (2010) Differences in the expression of endogenous efflux transporters in MDR1-transfected versus wildtype cell lines affect P-glycoprotein mediated drug transport. Br J Pharmacol 160(6):1453–1463
91. Nanayakkara AK et al (2018) Targeted inhibitors of P-glycoprotein increase chemotherapeutic-induced mortality of multidrug resistant tumor cells. Sci Rep 8(1):967
92. Uchida Y et al (2014) Blood-brain barrier pharmacoproteomics-based reconstruction of the in vivo brain distribution of P-glycoprotein substrates in cynomolgus monkeys. J Pharmacol Exp Ther 350(3):578–588
93. Huttunen KM et al (2022) Pharmacoproteomics of brain barrier transporters and substrate design for the brain targeted drug delivery. Pharm Res 39(7):1363–1392
94. Uchida Y et al (2020) Abundant expression of OCT2, MATE1, OAT1, OAT3, PEPT2, BCRP, MDR1, and xCT transporters in blood-arachnoid barrier of pig and polarized localizations at CSF- and blood-facing plasma membranes. Drug Metab Dispos 48(2):135–145
95. Uchida Y et al (2020) Comparison of absolute protein abundances of transporters and receptors among blood-brain barriers at different cerebral regions and the blood-spinal cord barrier in humans and rats. Mol Pharm 17(6):2006–2020
96. Jain S, Grandits M, Ecker GF (2018) Interspecies comparison of putative ligand binding sites of human, rat and mouse P-glycoprotein. Eur J Pharm Sci 122:134–143
97. Takeuchi T et al (2006) Establishment and characterization of the transformants stably-expressing MDR1 derived from various animal species in LLC-PK1. Pharm Res 23(7):1460–1472
98. Bundgaard C, Jensen CJ, Garmer M (2012) Species comparison of in vivo P-glycoprotein-mediated brain efflux using mdr1a-deficient rats and mice. Drug Metab Dispos 40(3):461–466
99. Kido Y et al (2001) Functional relevance of carnitine transporter OCTN2 to brain distribution of L-carnitine and acetyl-L-carnitine across the blood-brain barrier. J Neurochem 79(5):959–969
100. Okura T et al (2008) Involvement of the pyrilamine transporter, a putative organic cation transporter, in blood-brain barrier transport of oxycodone. Drug Metab Dispos 36(10):2005–2013

101. Chapy H et al (2015) A polyspecific drug/proton antiporter mediates diphenhydramine and clonidine transport at the mouse blood-retinal barrier. Br J Pharmacol 172(19):4714–4725
102. Ohashi R et al (1999) Na(+)-dependent carnitine transport by organic cation transporter (OCTN2): its pharmacological and toxicological relevance. J Pharmacol Exp Ther 291:778–84
103. Ishida K, Takaai M, Hashimoto Y (2006) Pharmacokinetic analysis of transcellular transport of quinidine across monolayers of human intestinal epithelial Caco-2 cells. Biol Pharm Bull 29(3):522–526
104. Luptakova D et al (2021) Neuropharmacokinetic visualization of regional and subregional unbound antipsychotic drug transport across the blood-brain barrier. Mol Psychiatry 26(12):7732–7745